Raman and optical spectroscopic studies of small-to-large polaron crossover in the perovskite manganese oxides

S. Yoon, H. L. Liu, G. Schollerer, and S. L. Cooper
Department of Physics and Frederick Seitz Materials Research Laboratory, University of Illinois at Urbana-Champaign, Urbana, Illinois 61801

P. D. Han and D. A. Payne
Department of Material Science and Engineering and Frederick Seitz Materials Research Laboratory, University of Illinois at Urbana-Champaign, Urbana, Illinois 61801

S.-W. Cheong
Bell Laboratories, Lucent Technologies, Murray Hill, New Jersey 07974

Z. Fisk
Department of Physics and National High Magnetic Field Laboratory, Florida State University, Tallahassee, Florida 32306
(Received 19 December 1997; revised manuscript received 12 March 1998)

We present an optical reflectance and Raman-scattering study of the $A_{1-x}A'_xMnO_3$ system as a function of temperature and doping ($0.2 \leqslant x \leqslant 0.5$). The metal-semiconductor transition in the $A_{1-x}A'_xMnO_3$ system is characterized by a change from a diffusive electronic Raman-scattering response in the high-temperature paramagnetic phase, to a flat continuum scattering response in the low-temperature ferromagnetic phase. We interpret this change in the scattering response as a crossover from a small-polaron-dominated regime at high temperatures to a large-polaron-dominated low-temperature regime. Interestingly, we observe evidence for the coexistence of large and small polarons in the low-temperature ferromagnetic phase. We contrast these results with those obtained for EuB_6, which is a low-T_c magnetic semiconductor with similar properties to the manganites, but with a substantially reduced carrier density and polaron energy. [S0163-1829(98)02429-1]

I. INTRODUCTION

The recent resurgence of interest in the so-called ''colossal'' magnetoresistance (CMR) compounds,[1,2] most notably the hole-doped manganese perovskites $A_{1-x}A'_xMnO_3$ (A = La, Pr, Nd; A' = Ca, Sr, Ba, Pb), has been motivated not only by the potential technological usefulness of these materials, e.g., as magnetic recording heads and magnetic-field sensors, but also by a desire to understand the complex physical properties that characterize this interesting class of strongly correlated materials.

The $A_{1-x}A'_xMnO_3$ system exhibits a rich phase diagram as one introduces carriers into the $x=0$ material by substituting divalent cations such as Ca, Sr, and Ba for trivalent La, Pr, or Nd. The parent material $AMnO_3$ is an antiferromagnetic insulator. However, for sufficiently large doping ($0.2 \leqslant x \leqslant 0.5$), these materials are ferromagnetic (FM) metals at low temperatures, with abrupt transitions to a paramagnetic (PM) semiconductor state above a doping-dependent Curie temperature which can be as high as $T_c \approx 350$ K for $x \sim 0.4$. T_c has also been shown to depend on the average ionic radius of the A site $\langle r_A \rangle$.[3] The remarkable magnetotransport properties of these materials have long been believed to result largely from the nature of the Mn d orbitals. Jonker and van Santen[4,5] pointed out that the substitution of divalent cations such as Ca and Sr in $AMnO_3$ causes a corresponding number of Mn atoms to change from Mn^{3+} to Mn^{4+}. Consequently, in $A_{1-x}A'_xMnO_3$ there are $(4-x)$ Mn d electrons, three of which occupy the t_{2g} levels, d_{xy}, d_{yz}, and d_{zx}, providing a strongly localized core spin of $S_c = 3/2$. The remaining $(1-x)$ electron occupies the e_g level with its spin oriented parallel to the core spin due to a strong Hund's rule exchange coupling J_H. In the so-called ''double-exchange'' model,[6] Zener suggested that transport in the FM metal phase involves hopping of the spin-polarized charge between Mn^{3+} and Mn^{4+} sites, thereby accounting for both ferromagnetism and metallic conduction in the low-temperature phase.

However, Millis *et al.*[7] recently argued that the double-exchange model alone is insufficient to account either for the low transition temperature or for the large change in resistivity through T_c in these materials. They propose that in addition to the double-exchange mechanism, strong electron-phonon coupling in the form of dynamical Jahn-Teller distortions tend to localize the conduction electrons in polaronic states. In this description, the phase diagram at low doping ($x \leqslant 0.5$) in $A_{1-x}A'_xMnO_3$ is primarily controlled by an effective coupling parameter λ which reflects the competition between the Jahn-Teller distortion energy and the carrier hopping energy. Notably, the presence of strong electron-phonon coupling and lattice polaron behavior in these materials has been deduced from a number of recent experimental results, including the large oxygen isotope shift of T_c,[8] structure in the Mn K edge obtained in x-ray-absorption fine-structure measurements,[9] the pair-distribution function resulting from neutron-scattering measurements,[10] and the temperature dependence of Hall coefficient and thermopower measurements.[11] Yet, in spite of this evidence, the interplay between lattice and magnetic contributions to CMR is still poorly understood.

In this paper we present optical reflectance and Raman-

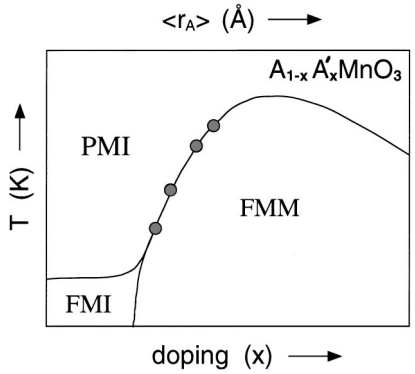

FIG. 1. Qualitative temperature-doping/ionic radius phase diagram for the $A_{1-x}A'_xMnO_3$ system, adapted from Ref. 3. The approximate T_c's of samples studied are indicated as filled circles. PMI is the paramagnetic insulator, FMI is the ferromagnetic insulator, and FMM is the ferromagnetic metal.

scattering results on the manganese perovskites as a function of temperature and doping (T_c, $\langle r_A \rangle$). Raman scattering, in particular, is a useful probe of materials in which there is a strong interplay between the electron, lattice, and spin dynamics, as this technique affords a means by which energy and symmetry information regarding phononic, electronic, and spin excitations can be simultaneously explored. Our results show strong evidence for a transition between a small-polaron-dominated PM phase and a large-polaron-dominated FM state in the $A_{1-x}A'_xMnO_3$ system. However, we also find evidence for the persistence of localized states even in the low-temperature metallic phase, suggesting that large and small polarons coexist in the FM phase of these materials. In an attempt to identify key features common to all colossal magnetoresistance materials, we also juxtapose our results for the $A_{1-x}A'_xMnO_3$ system with those for EuB_6, a low T_c magnetic semiconductor that exhibits similar physics to the manganites, but with a substantially reduced carrier density and polaron energy.

II. EXPERIMENT

Optical reflectance and Raman-scattering measurements were performed on both as-grown and mechanically polished (100) surfaces of single-crystalline $Pr_{0.7}Pb_{0.21}Ca_{0.09}MnO_3$ ($T_c \approx 145$ K), $La_{0.64}Pb_{0.36}MnO_3$ ($T_c \approx 200$ K), $La_{0.66}Pb_{0.23}Ca_{0.11}MnO_3$ ($T_c \approx 280$ K), and $Pr_{0.63}Sr_{0.37}MnO_3$ ($T_c \approx 300$ K). The location of these T_c values on a qualitative temperature-doping phase diagram for the $A_{1-x}A'_xMnO_3$ system is illustrated in Fig. 1. Raman-scattering and optical measurements were also performed on the (100) surfaces of EuB_6 single crystals prepared from an aluminum flux.

Optical reflectance measurements between 100 and 16 000 cm^{-1} (12 meV–2 eV) were obtained in a near-normal incidence configuration with a rapid scanning interferometer. The modulated light beam from the interferometer was focused onto either the sample or an Au reference mirror, and the reflected beam was directed onto a detector appropriate for the frequency range studied. The different sources, polarizers, and detectors used in these studies provided substantial spectral overlap, and the reflectance mismatch between adjacent spectral ranges was less than 1%.

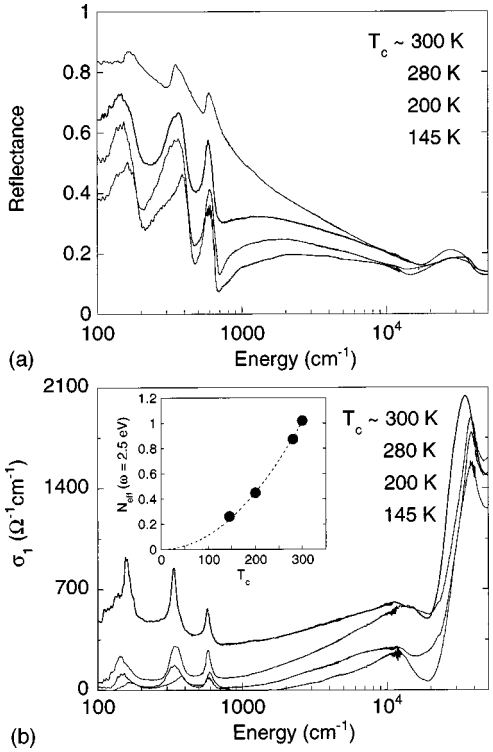

FIG. 2. (a) Room-temperature optical reflectance data of $A_{1-x}A'_xMnO_3$ for various T_c values. (b) Real part of room-temperature optical conductivity data of conductivity of $A_{1-x}A'_xMnO_3$ for various T_c's. Inset: $N_{\rm eff}(\omega=2.5\ {\rm eV})$ for the $A_{1-x}A'_xMnO_3$ samples studied [see Eq. (1) in the text].

Temperature-dependent Raman-scattering measurements were performed using a variable-temperature He cryostat and a Spex Triplemate spectrometer equipped with a nitrogen-cooled charge-coupled device (CCD) array detector. The samples were excited with 25 mW of the 5145-Å line of the argon laser. The spectra were obtained with the incident and scattered light polarized in the following configurations in order to identify the symmetries of the excitations studied: $(\mathbf{E}_i,\mathbf{E}_s)=(\mathbf{x},\mathbf{x})$: A_g; $(\mathbf{E}_i,\mathbf{E}_s)=(\mathbf{x},\mathbf{y})$: B_{1g}; $(\mathbf{E}_i,\mathbf{E}_s)=(\mathbf{x}+\mathbf{y},\mathbf{x}+\mathbf{y})$: A_g+B_{1g}; $(\mathbf{E}_i,\mathbf{E}_s)=(\mathbf{x}+\mathbf{y},\mathbf{x}-\mathbf{y})$: A_g(weak) $+B_{1g}$(weak); where $\mathbf{E}_i$ and $\mathbf{E}_s$ are the incident and scattered electric-field polarizations, respectively, $\mathbf{x}$ and $\mathbf{y}$ are the [100] and [010] crystal directions, respectively, and where $A_g(\Gamma_1^+)$ and $B_{1g}(\Gamma_3^+)$ are the singly degenerate irreducible representations of the $Pr_{0.7}Pb_{0.21}Ca_{0.09}MnO_3$, $La_{0.64}Pb_{0.36}MnO_3$, $La_{0.66}Pb_{0.23}Ca_{0.11}MnO_3$, and $Pr_{0.63}Sr_{0.37}MnO_3$ space group (D_{2h}^{16}-$Pnma$).

III. RESULTS AND DISCUSSION

A. Reflectance measurements

We first consider the effects of doping on the $A_{1-x}A'_xMnO_3$ system, as characterized by optical measurements. Figure 2 shows the room-temperature optical reflectance and conductivity of the $A_{1-x}A'_xMnO_3$ samples, illustrating the effects of doping and changing T_c ($\langle r_A \rangle$) on the low-frequency optical response. The reflectance of the highest T_c (≈ 300 K) crystal is over 70% for $\omega < 600$ cm^{-1}. As the frequency increases, the reflectance drops steadily

throughout the infrared, with a reflectance minimum near 18 000 cm^{-1}. Several electronic features are observed for frequencies above 18 000 cm^{-1}. With decreased doping, and a corresponding systematic reduction in T_c from 300 to 145 K, the reflectance in the entire infrared region decreases. As a consequence, the three infrared-active phonons observed are more pronounced in lower T_c samples. However, doping has little effect on the frequency of the reflectance minimum. A similar doping dependence has been reported previously in reflectance measurements of single crystalline $La_{1-x}Sr_xMnO_3$ ($0 \leqslant x \leqslant 0.3$) (Ref. 12) and polycrystalline $La_{1-x}Ca_xMnO_3$ ($0 \leqslant x \leqslant 1.0$).[13]

The real part of the optical conductivity, $\sigma_1(\omega)$, calculated from a Kramers-Kronig analysis of the reflectance curves, is presented at the bottom of Fig. 2. All the phonon modes and the electronic bands seen in the reflectance spectra are more easily resolved in the $\sigma_1(\omega)$ spectra. For all doping levels studied, we observe three phonon resonances at $\sim$150, 340, and 580 cm^{-1}, which are associated with the external mode of the rare earth-ions, and the bending and stretching modes of the MnO_6 octahedra,[14,15] respectively. The position and intensity of these phonon peaks are perturbed to some extent by both Ca doping and Pr substitution at the La sites, reflecting changes in the environments surrounding the MnO_6 octahedra.

As observed previously,[12,13] the low-frequency optical conductivity does not show a pronounced Drude-like response typical of a good metal in any of the samples studied. Rather, with decreasing T_c, the reflectance spectra of these materials changes from a spectrum typical of a poor conductor at higher doping ($T_c \approx 300$ K) to one typical of an insulator at lower doping ($T_c \approx 145$ K). In the model of Millis *et al.*,[16] this dramatic change in the optical response with decreasing T_c is attributed to the increased importance of electron-phonon coupling, and the attendant increased propensity for carrier localization, with decreased doping. At higher frequencies, we also observe two electronic absorption bands at $\sim$10 000 cm^{-1} and at $\sim$35 000 cm^{-1}, observed previously in $LaMnO_3$.[13,17] The doping dependence of the low-frequency conductivity of these samples can be summarized by plotting the integrated spectral weight in the conductivity,

$$\left[\frac{m}{m^*}\right] N_{\mathrm{eff}}(\omega) = \frac{2mV_{\mathrm{cell}}}{\pi e^2} \int_0^{\omega} \sigma_1(\omega')\, d\omega', \tag{1}$$

where $[m/m^*]N_{\mathrm{eff}}(\omega)$ is the effective number of carriers contributing to the conductivity below the frequency ω, m, and e are the bare electron mass and charge, respectively, m^* is the renormalized electron mass, and V_{cell} is the unit-cell volume. In the $A_{1-x}A'_xMnO_3$ materials, N_{eff} can be related to an effective squared plasma frequency via the relationship $\omega_p^2 \sim 6N_{\mathrm{eff}}$. The inset of Fig. 2 shows the quantity $N_{\mathrm{eff}}(\omega = 20\,000\ cm^{-1})$ plotted as a function of T_c, illustrating the correlation between the number of carriers and T_c in the $A_{1-x}A'_xMnO_3$ system.

B. Raman scattering

1. Paramagnetic phase

For the temperature dependence of the electronic response of $A_{1-x}A'_xMnO_3$, we turn to the results of Raman-scattering measurements. As shown in Fig. 3, the Raman-scattering response in the PM phase of all $A_{1-x}A'_xMnO_3$ samples is characterized by three phonon bands, a diffusive low-frequency electronic response, and a high-frequency electronic scattering peak near 1100 cm^{-1}. The Raman response in all samples can be well fit with the spectral response,

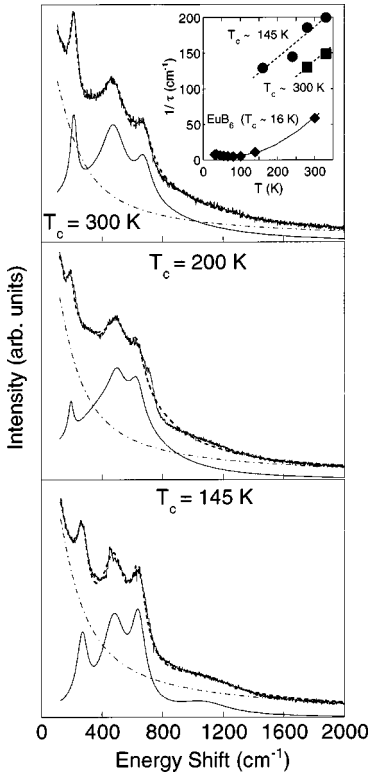

FIG. 3. Room-temperature Raman-scattering spectra of $A_{1-x}A'_xMnO_3$ samples. The dashed line is a fit to the data, which is a sum of inelastic (solid line) and diffusive (dashed-dotted line) responses [see Eqs. (3) and (4)]. Inset: Scattering rates in $A_{1-x}A'_xMnO_3$ and EuB_6, illustrating the linear increase of the scattering rate with temperature for the $A_{1-x}A'_xMnO_3$ samples studied.

$$S(\omega) = S_{\mathrm{ph}}(\omega) + S_{\mathrm{el}}(\omega), \tag{2}$$

where

$$S_{\mathrm{ph}}(\omega) = [1 + n(\omega)] \sum_{i=1}^{3} \frac{A_i \omega \Gamma_i}{(\omega^2 - \omega_i^2)^2 + \omega^2 \Gamma_i^2} \tag{3}$$

represents three phonon modes with associated mode frequency, ω_i, linewidth, Γ_i, and amplitude A_i, and

$$S_{\mathrm{el}}(\omega) = [1 + n(\omega)] \left[\frac{A\omega/\tau}{\omega^2 + 1/\tau^2} + \frac{A_{\mathrm{el}} \omega \Gamma_{\mathrm{el}}}{(\omega^2 - \omega_{\mathrm{el}}^2)^2 + \omega^2 \Gamma_{\mathrm{el}}^2} \right] \tag{4}$$

is the electronic contribution to the spectrum, consisting of a ''collision-dominated'' low-frequency response (dashed-dotted line) associated with diffusive hopping of the carriers with a scattering rate $\gamma = 1/\tau$, and a high-frequency inelastic electronic contribution near $\omega_{\mathrm{el}} \sim 1000 - 1100\ cm^{-1}$, which is most clearly observable at low temperatures and in the lower T_c materials. The quantity $[1 + n(\omega)] = [1 - \exp(-\hbar\omega/k_BT)]^{-1}$ is the Bose-Einstein thermal factor.

Considering first the phonon response in Fig. 3, the three observed Raman-active phonon bands near ~ 200, ~ 470, and $\sim 630\ \mathrm{cm}^{-1}$ have frequencies consistent[18] with the rare-earth vibrational mode, the Mn-O bending mode, and the Mn-O stretch mode, respectively. Notably, as no Raman-active phonon modes are anticipated in the perovskite structure, O_h^1-$Pm3m$, the presence of Raman modes in Fig. 3 is indicative of symmetry-breaking due to local distortions in these materials. Indeed, the Mn-O modes are significantly broader than the rare-earth mode, consistent with the general belief that the disorder in these systems is primarily associated with the MnO_6 octahedra. Interestingly, we find that near T_c, the Mn-O bending and stretch modes narrow and intensify substantially with decreasing temperature, suggesting that the MnO_6 octahedra becomes more ordered below T_c, in agreement with other observations.[10,19,20] For example, we find that the Mn-O stretch mode narrows with decreasing temperature by $\Delta\Gamma/\Gamma \sim 12$, 30, and 16% in the $T_c \approx 145$, 200, and 300 K samples, respectively.[21] Similar, though less pronounced, evidence for lattice disorder associated with the boron octahedra is also observed in EuB_6.[22]

As mentioned above, the electronic Raman-scattering response in the PM phase of the manganites is dominated by (a) a diffusive low-frequency scattering response described by the first term in Eq. (4), which is associated with incoherent hopping of the carriers, and (b) a high-frequency inelastic-scattering response with a doping-dependent peak energy near $\omega_{\mathrm{el}} \sim 100-1100\ \mathrm{cm}^{-1}$, described by the second term in Eq. (4). Interestingly, the diffusive scattering response in the PM phase of the $A_{1-x}A'_xMnO_3$ is quite similar to that observed in the PM phase of EuB_6,[23] but with a substantially larger scattering rate due to greater disorder (inset, Fig. 3). As a function of decreasing temperature in the PM phase, the inset of Fig. 3 shows that the carrier scattering rate in the $A_{1-x}A'_xMnO_3$ system decreases roughly linearly with temperature. As the strong lattice disorder in these materials is the dominant carrier scattering mechanism in the PM phase, this trend likely reflects the reduction of lattice disorder with decreasing temperature in the manganites (see, for example, Refs. 10, 19, and 20).

Figure 4 shows the temperature dependence of the Raman spectrum for the $T_c \approx 145$, 200, and 300 K samples. As a function of decreasing temperature in the PM phase, the high-frequency inelastic peak gains scattering intensity at the expense of intensity in the diffusive scattering response. Additionally, there is a more dramatic change in the electronic scattering response through the metal-semiconductor transition, characterized by a loss of the diffusive response, which we will discuss in greater detail in the next section. The growth of intensity in the high-frequency electronic scattering response with reduced temperature in the PM phase is shown more clearly in Fig. 5, which plots the high-frequency scattering response of the $T_c \approx 145$ K sample after removing the diffusive and phonon contributions. Two noteworthy interpretations of the high-frequency inelastic-scattering contribution are consistent with its temperature and frequency dependence: (1) A transition between Jahn-Teller split $e_{g\uparrow}^1$ and $e_{g\uparrow}^2$ levels, which is expected to be Raman active.[24] This interpretation is unlikely for several reasons. First, the observed energy of the electronic Raman excitation at ω_{el}

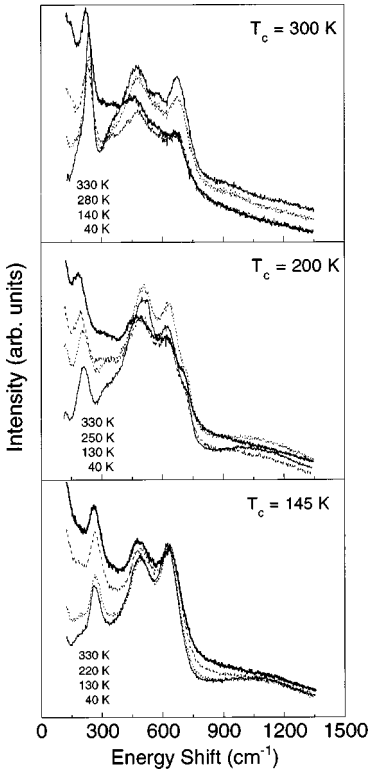

FIG. 4. The temperature dependence of the Raman spectra of $A_{1-x}A'_xMnO_3$. The laser heating effect on the sample temperature has been taken into account.

$\sim 1100\ \mathrm{cm}^{-1}$ (0.14 eV) is substantially smaller than band-structure estimates of the Jahn-Teller splitting, ~ 2.4 eV,[25] or even the more favorable estimates of Millis, ~ 0.6 eV.[24,26] Second, calculations suggest that the Jahn-Teller splitting should be strongly temperature dependent, while the peak at ω_{el} is not highly sensitive to temperature (see Fig. 5). (2) A more reasonable possibility is that the high-frequency Raman-scattering peak is associated with photoionization of small polarons, i.e., a transition from a band of localized small polaron states present in the PM phase[10,11] to the conduction band. There are currently no models for electronic Raman scattering from small polarons, but an estimate of the

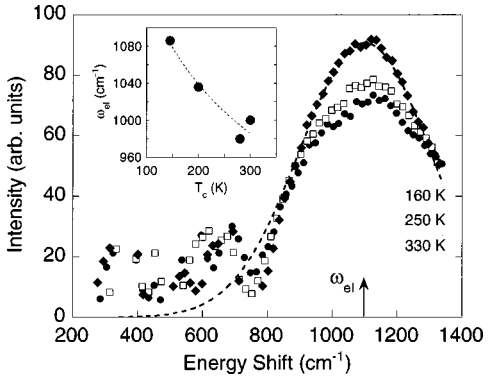

FIG. 5. The high-frequency Raman-scattering spectrum of the $T_c \approx 145$ K sample after removing the diffusive and phonon contributions. The dashed line is a fit to the data using the small-polaron response given by Eq. (5) in the text. The inset illustrates that the peak position (small-polaron photoionization energy) shifts systematically to lower energy with increased T_c.

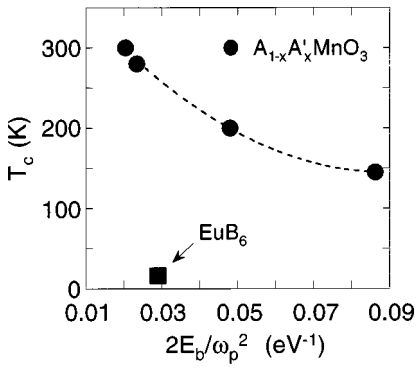

FIG. 6. T_c vs $2E_b/\omega_p^2$ for $A_{1-x}A'_xMnO_3$ (filled circle), where E_b is the polaron binding energy and ω_p is the plasma frequency, illustrating a systematic decrease in $2E_b/\omega_p^2$ with increasing T_c. The quantity $2E_b/\omega_p^2$ estimated for EuB_6 is also shown for comparison (filled square).

high-frequency scattering response which provides a qualitative description of the data is $S(\omega,T)\sim\omega\sigma_{\rm sp}(\omega,T)$, where[27]

$$\sigma_{\rm sp}(\omega,T)=\sigma(0,T)\,\frac{\sinh(4E_b\hbar\omega/\Delta^2)}{4E_b\hbar\omega/\Delta^2}\exp[-(\hbar\omega)^2/\Delta^2] \tag{5}$$

is the small-polaron optical conductivity, E_b is the small-polaron binding energy, $\sigma(0,T)$ is the dc conductivity, $\Delta=2\sqrt{2E_bE_{\rm vib}}$ is a broadening factor, and $E_{\rm vib}$ is the characteristic vibrational energy, which is $E_{\rm vib}=k_BT$ in the high-temperature regime and $E_{\rm vib}=\hbar\omega_{\rm ph}/2$ at low temperatures. In this description, the diffusive low-frequency scattering response in Figs. 3 and 4 is associated with incoherent hopping of self-trapped carriers between localized sites, and the high-frequency inelastic excitation is associated with the photoionization of the small polaron, with an energy given by $\hbar\omega_{\rm el}=2E_b$ for sufficiently strong electron-phonon coupling. Several features of this scattering peak support the small-polaron interpretation. First, the small-polaron picture provides a reasonable fit to the high-frequency scattering response (dashed line in Fig. 5), with a value for the polaron formation energy, $\hbar\omega_{\rm el}=2E_b\sim138$ meV which is within 30% of the value estimated from thermopower measurements.[11] Additionally, Fig. 5 shows that this peak has a temperature-dependence characteristic of small-polaron photoionization, increasing with decreasing temperature at the expense of the diffusive scattering strength. Finally, the peak position shifts systematically to lower energy with increased T_c (inset). This trend occurs as a much weaker function of inverse carrier density than in Thomas-Fermi screening, for example, but is nevertheless consistent with the expected decrease in polaron binding energy with doping.

Interestingly, one can use the polaron binding energy values obtained from these Raman results with the optical reflectance measurements of the squared plasma frequency ω_p^2 to estimate the ratio of the polaron binding energy to the electron hopping energy. Figure 6 plots T_c vs $2E_b/\omega_p^2$ for the $A_{1-x}A'_xMnO_3$ samples measured, showing a systematic decrease in this quantity with increasing T_c, in qualitative agreement with the phase diagram of Millis *et al.*[16] Notably, a similar estimate of this quantity in EuB_6, using measurements of the polaron energy from earlier Raman studies,[23]

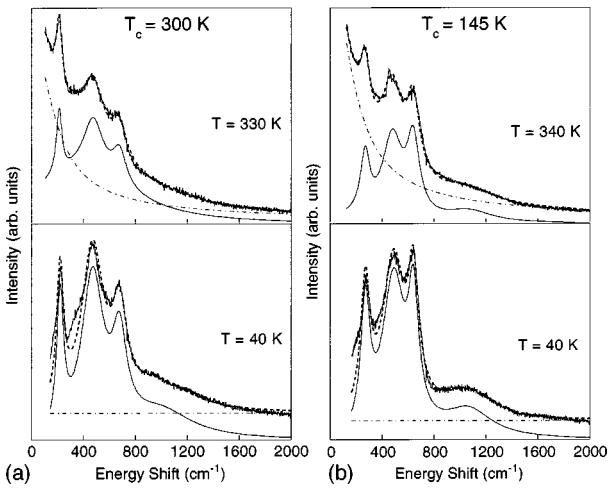

FIG. 7. The Raman-scattering spectra in both the PM and FM phases for (a) the $T_c\approx300$ K sample and (b) $T_c\approx145$ K sample. The dotted line is a fit to the data which is a sum of the solid line and the dashed-dotted line [see Eqs. (3) and (4), and the discussion thereafter].

show that this material exhibits a ratio of polaron and electron hopping energies which is comparable to that in the manganites, albeit with substantially reduced values for ω_p and E_b. This suggests that the similarity in the observed spectral response of EuB_6 and the doped manganites may not be accidental, but rather reflects a fundamental similarity in the competition between the polaron formation and carrier kinetic energies in these two systems.

2. Metal-semiconductor transition and ferromagnetic phase

The low-frequency Raman-scattering response in the $A_{1-x}A'_xMnO_3$ system exhibits a distinctive change through the PM semiconductor/FM metal transition, characterized by a change from a diffusive scattering response [first term in Eq. (4)], to a flat continuum response which is typical of electronic scattering observed in strongly correlated metallic oxides such as $La_{1-x}Sr_xTiO_3$ (Ref. 28) and the high-T_c cuprates.[29] This crossover is best illustrated in Fig. 7, which compares the fitted Raman response in both the PM and FM phases for the $T_c\approx300$ K and $T_c\approx145$ K samples. The crossover between these two regimes is also shown for the $T_c\approx145$ K sample in Fig. 8, which compares the temperature dependence of the integrated scattering strength ratio for the diffusive response, $I_{\rm diff}({\rm T})/I_{\rm diff}({\rm T}=350\ {\rm K})$, and the flat continuum response, $I_{\rm cont}({\rm T})/I_{\rm cont}({\rm T}=90\ {\rm K})$. Similar results were obtained for the other samples measured. Notably, the transition between diffusive and metallic regimes near T_c in $A_{1-x}A'_xMnO_3$ is quite similar to that observed in the lower T_c material, EuB_6, as can be seen in the comparison in Fig. 9, where the inelastic contributions to the response in $A_{1-x}A'_xMnO_3$ have been removed for comparison. However, while EuB_6 exhibits an extremely abrupt transition between these regimes, the transition in $A_{1-x}A'_xMnO_3$ occurs more gradually below T_c, consistent with optical results which show a continuous evolution of a Drude response below T_c.[12]

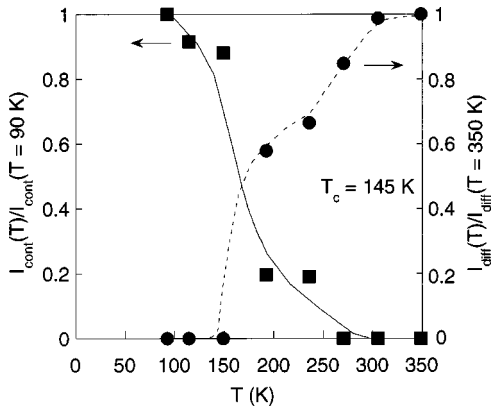

FIG. 8. The temperature dependence of the integrated scattering strength ratio for the diffusive response, $I_{\mathrm{diff}}(\mathrm{T})/I_{\mathrm{diff}}(\mathrm{T}=350\ \mathrm{K})$ (filled circles), and the flat continuum response, $I_{\mathrm{cont}}(\mathrm{T})/I_{\mathrm{cont}}(\mathrm{T}=90\ \mathrm{K})$ (filled squares) for the $T_c \approx 145$ K sample.

Two theoretical descriptions of FM metal/PM semiconductor transition in magnetic semiconductors are particularly noteworthy with regard to these results. Hillery *et al.*[30] attribute the MI transition in EuO to a collapse of large-radius polarons due to the increase of spin disorder with increasing temperature. This picutre appears to capture the physics of the abrupt MI transition observed in EuB_6.[23] On the other hand, Millis *et al.*[7] interpret the decreased electron itineracy in the high-temperature phase of $A_{1-x}A'_xMnO_3$ to a decrease in the electron hopping parameter t, relative to the self-trapping energy of a Jahn-Teller polaron. The dramatically different scattering responses in the FM and PM phases in Fig. 7 are indeed consistent with a crossover from a metallic low-temperature regime to a small-polaron-dominated high-temperature regime. However, this crossover occurs gradually below T_c in the manganese perovskites, in contrast with the rather abrupt crossover apparent in the electronic Raman response of EuB_6. This likely reflects the fact that both the carrier bandwidth t, governed by the double-exchange mechanism, and the spin-dependent electron-phonon coupling change gradually with temperature below T_c in the manganese oxide CMR materials.[16]

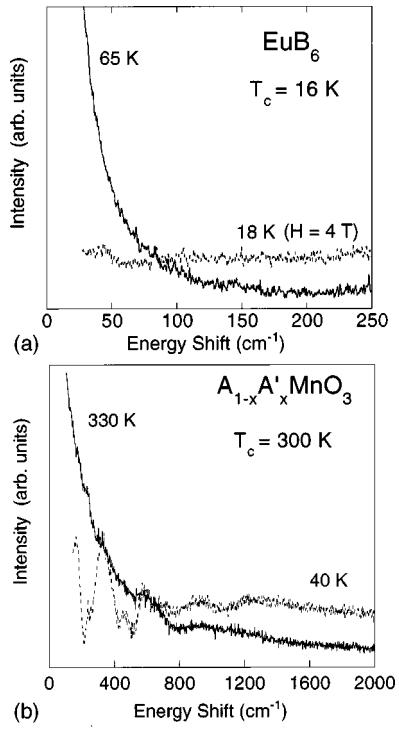

FIG. 9. The high-temperature diffusive response compared with the flat, low-temperature metallic response in both (a) $A_{1-x}A'_xMnO_3$, after removing the inelastic contributions, and (b) EuB_6.

Importantly, while the transition to the FM phase in $A_{1-x}A'_xMnO_3$ is associated with the development of a dominant metallic response, there is evidence that localized states persist in the FM metal phase down to the lowest temperatures measured. Indeed Fig. 7 illustrates that the flat metallic scattering response coexists with a remnant of the high-energy ($\omega_{\mathrm{el}} \sim 1100\ \mathrm{cm}^{-1}$) inelastic peak associated with the ionization energy of small polarons. One possibility is that this residual peak is due to the presence of surface strains in the samples, although we feel that this possibility is less likely since we find that the polaron feature persists at low temperatures in samples with both mechanically polished and as-grown surfaces. A more likely possibility is that this residual peak reflects ''two-fluid'' behavior in the low-temperature FM phase of $A_{1-x}A'_xMnO_3$ wherein mobile ''large polarons'' coexist with carriers that remain localized by structural disorder in the FM phase. Low-temperature thermopower measurements, which reveal an exponentially decreasing thermopower in the FM phase of $A_{1-x}A'_xMnO_3$ indicative of unsaturated ferromagnetism,[11] also appear to be consistent with this possibility. Interestingly, it is clear from Fig. 7 that there is an increase in the fraction of total electronic spectral weight associated with the small-polaron response in the FM phase with decreasing T_c, in particular, $I_{\mathrm{pol}}/I_{\mathrm{total}} \sim 0.55$ and 0.65 in the $T_c \approx 300$ and 145 K samples, respectively. This result likely reflects the increased polaron binding energy, and increased lattice disorder, in lower T_c materials, resulting in the binding of a larger fraction of the carriers at low temperatures.

IV. CONCLUSIONS

In summary, we observe spectroscopic evidence for small polarons in the high-temperature paramagnetic phase of the $A_{1-x}A'_xMnO_3$ system, and estimate a polaron photoionization energy of roughly 140 meV for the $T_c \sim 145$ K sample. Furthermore, we find that the metal-semiconductor (MS) transition in the manganese perovskites is characterized by a change in the electronic Raman-scattering spectrum from a diffusive response in the PM phase to a flat continuum response in the FM regime. This dramatic change in scattering response reflects a fundamental change from small-polaron-dominated transport in the PM phase to large-polaron (metallic) transport in the FM phase. Significantly, we also find evidence that large and small polarons coexist in the low-temperature phase of the $A_{1-x}A'_xMnO_3$ system, due possibly to the presence of lattice disorder which localizes a fraction of the carriers even in the FM phase. This behavior distinguishes the $A_{1-x}A'_xMnO_3$ system from magnetic semiconductors such as EuB_6 and EuO in which the FM metallic state is fully polarized due to the complete disappearance of spin disorder at the FM transition.[23,30] Finally, we find that

the low-T_c magnetic semiconductor EuB_6 ($T_c \approx 16$ K) exhibits a temperature-dependent Raman-scattering response that is similar to the manganese perovskites studied, but with a substantially reduced carrier density, scattering rate, and polaron energy. While the carrier hopping mechanisms are clearly different in the $A_{1-x}A'_xMnO_3$ and EuB_6 systems, both were estimated to have a comparable ratio of polaron binding energy to carrier kinetic energy. This comparison suggests that T_c and the MS transition in these magnetic semiconductors are less influenced by specific details related to carrier hopping, e.g., the double-exchange mechanism, than by the general details governing the competition between polaron formation and carrier hopping that are common to these materials.

ACKNOWLEDGMENTS

This work was supported by the Department of Energy under Grant No. DEFG02-96ER45439 (S.Y., H.L.L, G.S., and S.L.C.) and by the NHMFL through Grant No. NSF DMR90-16241 (Z.F.). We would like to acknowledge use of the MRL Laser Lab Facility, where the Raman-scattering measurements were carried out. Z.F. also acknowledges support from the Japanese New Energy and Industrial Development Organization.

[1] S. Jin, T. H. Tiefel, M. McCormack, R. A. Fastnacht, R. Ramesh, and L. H. Chen, Science **264**, 413 (1994).
[2] R. von Helmolt, J. Wecker, B. Holzapfel, L. Schultz, and K. Samwer, Phys. Rev. Lett. **71**, 2331 (1993).
[3] H. Y. Hwang, S-W. Cheong, P. G. Radaelli, M. Marezio, and B. Batlogg, Phys. Rev. Lett. **75**, 914 (1995).
[4] G. H. Jonker and J. H. van Santen, Physica (Amsterdam) **16**, 337 (1950).
[5] J. H. van Santen and G. H. Jonker, Physica (Amsterdam) **16**, 599 (1950).
[6] C. Zener, Phys. Rev. **82**, 403 (1951); P. W. Anderson and H. Hasegawa, *ibid.* **100**, 675 (1955); P.-G. de Gennes, *ibid.* **118**, 141 (1960).
[7] A. J. Millis, P. B. Littlewood, and B. I. Shraiman, Phys. Rev. Lett. **74**, 5144 (1995).
[8] G. Zhao, K. Conder, H. Keller, and K. A. Müller, Nature (London) **381**, 676 (1996).
[9] T. A. Tyson, J. M. de Leon, S. D. Conradson, A. R. Bishop, J. J. Neumeier, H. Röder, and J. Zang, Phys. Rev. B **53**, 13 985 (1996).
[10] S. J. L. Billinge, R. G. DiFrancesco, G. H. Kwei, J. J. Neumeier, and J. D. Thompson, Phys. Rev. Lett. **77**, 715 (1996).
[11] M. Jaime, M. B. Salamon, M. Rubinstein, R. E. Treece, J. S. Horwitz, and D. B. Chrisey, Phys. Rev. B **54**, 11 914 (1996); M. Jaime, H. T. Hardner, M. B. Salamon, M. Rubinstein, P. Dorsey, and D. Emin, Phys. Rev. Lett. **78**, 951 (1997).
[12] Y. Okimoto, T. Katsufuji, T. Ishikawa, A. Urushibara, T. Arima, and Y. Tokura, Phys. Rev. Lett. **75**, 109 (1995); Y. Okimoto, T. Katsufuji, T. Ishikawa, T. Arima, and Y. Tokura, Phys. Rev. B **55**, 4206 (1997).
[13] J. H. Jung, K. H. Kim, D. J. Eom, T. W. Noh, E. J. Choi, J. Yu, Y. S. Kwon, and Y. Chung, Phys. Rev. B **55**, 15 489 (1997).
[14] K. H. Kim, J. Y. Gu, H. S. Choi, G. W. Park, and T. W. Noh, Phys. Rev. Lett. **77**, 1877 (1996).
[15] K. Li, X. Li, K. Zhu, J. Zhu, and Y. Zhang, J. Appl. Phys. **81**, 6943 (1997).
[16] A. J. Millis, R. Mueller, and B. I. Shraiman, Phys. Rev. B **54**, 5405 (1996).
[17] T. Arima and Y. Tokura, J. Phys. Soc. Jpn. **64**, 2488 (1995).
[18] M. N. Iliev, M. V. Abrashev, H.-G. Lee, V. N. Popov, Y. V. Sun, C. Thomsen, R. L. Mens, and C. W. Chu, Phys. Rev. B **57**, 2872 (1998).
[19] P. G. Radaelli, M. Marezio, H. Y. Hwang, S-W. Cheong, and B. Batlogg, Phys. Rev. B **54**, 8992 (1996).
[20] D. Louca and T. Egami, J. Appl. Phys. **81**, 5484 (1997).
[21] It should be noted, however, that we do not observe an abrupt change in phonon frequencies, in contrast to the infrared results of Kim *et al.* (Ref. 14).
[22] S. Yoon, P. Nyhus, and S. L. Cooper (unpublished).
[23] P. Nyhus, S. Yoon, M. Kauffman, S. L. Cooper, Z. Fisk, and J. Sarrao, Phys. Rev. B **56**, 2717 (1997).
[24] A. J. Millis, Phys. Rev. B **53**, 8434 (1996).
[25] S. Satpathy, Z. S. Popović, and F. R. Vukajlović, Phys. Rev. Lett. **76**, 960 (1996).
[26] R. Gupta, A. K. Sood, R. Mahesh, and C. N. R. Rao, Phys. Rev. B **54**, 14 899 (1996).
[27] D. Emin, Adv. Phys. **24**, 305 (1975).
[28] T. Katsufuji and Y. Tokura, Phys. Rev. B **49**, 4372 (1994).
[29] S. Sugai, Y. Enomoto, and T. Murakami, Solid State Commun. **72**, 1193 (1989).
[30] M. S. Hillery, D. Emin, and N. H. Liu, Phys. Rev. B **38**, 9771 (1988).